



ACADEMIC
PRESS

Available online at www.sciencedirect.com

SCIENCE @ DIRECT®

Journal of Magnetic Resonance 162 (2003) 250–258

JMR
Journal of
Magnetic Resonance

www.elsevier.com/locate/jmr

An improved gridding method for spiral MRI using nonuniform fast Fourier transform

Liewei Sha,^a Hua Guo,^b and Allen W. Song^{b,*}

^a Department of Electrical and Computer Engineering, Duke University, USA

^b Brain Imaging and Analysis, Center, Duke University Medical Center, Box 3918, Durham, NC 27710, USA

Received 30 August 2002; revised 11 February 2003

Abstract

The algorithm of Liu and Nguyen [IEEE Microw. Guided Wave Lett. 8 (1) (1998) 18; SIAM J. Sci. Comput. 21 (1) (1999) 283] for nonuniform fast Fourier transform (NUFFT) has been extended to two dimensions to reconstruct images using spiral MRI. The new gridding method, called LS_NUFFT, minimizes the reconstruction approximation error in the Least Square sense by generated convolution kernels that fit for the spiral k -space trajectories. For analytical comparison, the LS_NUFFT has been fitted into a consistent framework with the conventional gridding methods using Kaiser–Bessel gridding and a recently proposed generalized FFT (GFFT) approach. Experimental comparison was made by assessing the performance of the LS_NUFFT with that of the standard direct summation method and the Kaiser–Bessel gridding method, using both digital phantom data and in vivo experimental data. Because of the explicitly optimized convolution kernel in LS_NUFFT, reconstruction results showed that the LS_NUFFT yields smaller reconstruction approximation error than the Kaiser–Bessel gridding method, but with the same computation complexity.

© 2003 Elsevier Science (USA). All rights reserved.

Keywords: Spiral MRI; Reconstruction; NUFFT; LS_NUFFT; Gridding

1. Introduction

Spiral scanning in k -space for MRI [1,2] has received increased attention in functional brain imaging and cardiac imaging because of its efficient trajectory, low motion sensitivity, and high speed. In spiral MRI, the observed signal represents 2D Fourier transform of the object along a spiral trajectory in k -space. The object image can be reconstructed from spiral MRI signal using various algorithms.

A straightforward approach is the direct summation of the inverse Fourier transform of the spiral signal weighted by a proper density compensation function. Although the high computational demand of the direct summation method makes it impractical, it nevertheless provides a mathematical foundation to be used as a

standard to evaluate the reconstruction quality of other reconstruction algorithms.

The widely accepted Kaiser–Bessel gridding method [3,4] speeds up the reconstruction by interpolating the data onto a Cartesian grid using Kaiser–Bessel convolution kernel followed by fast inverse Fourier transform. However, the performance of the Kaiser–Bessel gridding method highly depends on the selection of the kernel function parameter β . And even by using the optimal parameter, the reconstructed image could still have trajectory-dependent local distortions.

Sarty et al. [6] have extended a NUFFT method of Dutt and Rokhlin [5] to spiral MRI, which is called GFFT. GFFT is actually equivalent to a convolution gridding method with a Gaussian kernel. Although it is claimed in [6] that GFFT has better performance than Kaiser–Bessel gridding method with a proper selection of the Gaussian kernel parameter for 64×64 pixel image, it is not consistently better for all image sizes. And the GFFT also highly depends on the selection of the kernel parameter. Therefore, those two methods are

* Corresponding author. Fax: 1-919-681-7033.

E-mail address: allen.song@duke.edu (A.W. Song).

both referred as “conventional gridding method” in this paper.

The LS_NUFFT is different from the conventional gridding method in that it does not use any ready-made kernel functions, but generates the kernel matrices that fit for the spiral trajectory in the sense of least square approximation error. Since those kernel matrices are customized to the specific trajectory, it is possible that the reconstruction performance could be improved than that of the noncustomized conventional gridding methods. Similar goal was achieved efficiently in a recent report [7] through a different approach using Min–Max criterion plus iterative reconstruction. As with the LS_NUFFT, since [8,9] have provided some important analytical solutions, the additional computational cost to obtain the kernel matrix is small and can be ignored.

In the following sections, the LS_NUFFT and conventional gridding methods are first compared analytically in the NUFFT framework. The performance of the LS_NUFFT was then evaluated experimentally against that of the direct summation and Kaiser–Bessel gridding methods, using simulated digital phantom data and in vivo experimental data for 64×64 and 128×128 pixel images.

2. Analytical assessment

2.1. Direct summation

Ideally, the reconstruction of the object image from its two-dimensional Fourier transform in the continuous k -space can be expressed as

$$I(x) = \int_k s(k) e^{i2\pi xk} dA, \quad x \in \text{FOV}, \quad (1)$$

where $x = (x, y)$ represents the location of the point in the reconstructed image. $k = (k_x, k_y)$ is the position of the k -space data point. $s(k)$ is the k -space data. dA represents the area associating with k . FOV is the field of view.

In practice, the real spiral data is collected on a discrete and finite grid of the k -space, along a spiral trajectory. Before making direct summation approximation, a density compensation function (DCF) corresponding to dA is necessary to enable effective uniform k -space density. There are several options to obtain DCF, including the Voronoi area approach [10], the method derived by Remi et al. in [11] and the method proposed by Meyer et al. in [12]. The DCF of Meyer et al. is used in this paper because it is accurate and computationally easy, and it works directly for both single-shot and multi-shot (interleaved) trajectories. This DCF is defined as

$$D(k) = |k'| |\sin(\arg\{k'\} - \arg\{k\})|, \quad (2)$$

where k' is the k -space velocity vector.

Therefore, the direct summation reconstruction as an approximation to Eq. (1) can be expressed as

$$I(x) \approx C \sum_{p=1}^M s(k_p) e^{i2\pi xk_p} D(k_p), \quad (3)$$

where p is the index of the data on the k -space trajectory. M is the number of k -space data points and C is the constant scaling factor.

To simplify later derivations, let $s_p = s(k_p)$, $D_p = D(k_p)$. Assume the FOV is located at $[-l/2, l/2] \times [-l/2, l/2]$, x can be re-scaled by a factor of $1/l$, so that $x, y \in [-1/2, 1/2]$. Specifically, assume that $x, y = [-N/2 : N/2 - 1]/N$, where N is the number of pixels along each axis of the reconstructed image. Simultaneously, k_p could be rescaled by a factor of l , so that the form of $I(x)$ does not change. since originally $k_p \in [-k_{\max}, k_{\max}]$ and $k_{\max} = N/2l$, after scaling, $k_{x_p}, k_{y_p} \in [-N/2, N/2]$.

The final form of the direct summation reconstruction is

$$I(x, y) = \sum_{p=1}^M s_p \exp(i2\pi(xk_{x_p} + yk_{y_p})) D_p, \quad (4)$$

where $x, y = [-N/2 : N/2 - 1]/N$ and $k_{x_p}, k_{y_p} \in [-N/2, N/2]$. The constant C is ignored for simplicity because it does not change the relative contrast of the reconstructed image.

Eq. (4) is used as a standard to compare the LS_NUFFT and conventional gridding approach in section 3.2.

2.2. Improved NUFFT

2.2.1. 1D NUFFT

The concept of NUFFT, as first stated by Dutt and Rokhlin [5], is to approximate the item e^{ixc} defined on nonuniform spaced point c by a finite set of items defined on uniform spaced points in the neighborhood of point c . Theorem 2.10 in [5] states:

Theorem 1. Let $b > 1/2$, $c, d > 0$ be real numbers, and let $m \geq 2$, $q \geq 4b\pi$ be integers, then for any $x \in [-d, d]$,

$$\left| e^{ixc} - s_x^{-1} \sum_{p=[cmd/\pi]-q/2}^{[cmd/\pi]+q/2} \rho_p e^{ipx/m} \right| < e^{-b\pi^2(1-1/m^2)}(4b+9), \quad (5)$$

where $[\cdot]$ is the round function. $[cmd/\pi]$ denotes the integer nearest to cmd/π . $s_x = \exp(-b(\pi x/md)^2)$ and $\rho_p = (2\sqrt{b\pi})^{-1} \exp(-(c-p)^2/4b)$. When this idea is extended to two dimensions for image reconstruction, ρ is equivalent to the kernel function in conventional gridding method. m represents the scaling factor of FOV. Setting m to 2 is the same as doubling the image FOV, which is proposed by O’Sullivan in [4] for gridding

method. And $q + 1$ represents the number of approximate items for each nonuniform spaced data point. q is the same as the parameter ‘window width’ used in conventional gridding method.

2.2.2. Improved 1D NUFFT

Liu and Nguyen have improved NUFFT by selecting better scaling factors, one of which is the cosine scaling factor $s_c(x) = \cos(\pi x/mN)$, and have proposed a better way to generate the kernel function ρ , which makes the following term minimum in the Least-Square sense,

$$\left\| s_c(x) e^{i2\pi c_p x} - \sum_{j=-q/2}^{q/2} \rho(j, c_p) e^{i2\pi(j+[mc_p])x/m} \right\|, \quad (6)$$

where $x = [-N/2 : N/2 - 1]/N$, N is the number of reconstructed points. $p = 1, \dots, M$, M is the number of nonuniform spaced frequency points. q is assumed to be an even number, c_p is a real number. $[\cdot]$ denotes the round function. It is not difficult to see that the above form is similar to the left part of Eq. (5) by considering that the latter takes $d = 1/2$, $c = 2\pi c_p$, $p = [cmd/\pi] + j = [mc_p] + j$ and $s_c(x)$ is the same as s_x , except that the kernel ρ in the above form is no longer a known function and needs to be solved. Note that since the kernel function for the improved NUFFT is optimally solved, it will be better than any other kernel function that uses the same scaling factor under the same Least-Square criterion. Yet the bound for the improved NUFFT has not been explicitly obtained as that for the NUFFT in [5].

The cosine scaling factor used in Liu and Nguyen’s report is adopted in this paper for the LS_NUFFT, which enables closed form solution for the kernel function. It is possible to find a better scaling factor to further improve the performance of the LS_NUFFT. According to Eqn.(4-9,12) in [8], the $(q + 1) \times M$ kernel matrix corresponding to the cosine scaling factor can be expressed as

$$\rho_{j,c_p} = \mathbf{G}_{j,k} a_{k,c_p}, \quad j, k = -\frac{q}{2} \dots \frac{q}{2}, \quad p = 1..M,$$

where

$$\mathbf{G} = \mathbf{F}^{-1}, \mathbf{F}_{j,k} = \frac{-2i \sin(\pi(j-k)/m)}{1 - \exp(i2\pi(j-k)/mN)},$$

$$a_{k,c_p} = i \sum_{\gamma=-1,1} \frac{\sin[\frac{\pi}{2m}(2k - \gamma - 2\{mc_p\})]}{1 - \exp(i\frac{\pi}{Nm}(2\{mc_p\} - 2k + \gamma))} \quad (7)$$

$$\{mc_p\} = mc_p - [mc_p].$$

2.2.3. LS_NUFFT

To this end, the improved 1D NUFFT is extended to the LS_NUFFT for spiral MRI. The target is to optimally approximate the form of direct summation reconstruction defined in Eq. (4).

The items in Eq. (4) are approximated by

$$\exp(i2\pi x k_{x_p}) \approx s_c(x)^{-1} \sum_{j1=-q/2}^{q/2} \rho_1(j1, k_{x_p}) \exp(i2\pi x ([mk_{x_p}] + j1)/m),$$

$$\exp(i2\pi y k_{y_p}) \approx s_c(y)^{-1} \sum_{j2=-q/2}^{q/2} \rho_2(j2, k_{y_p}) \exp(i2\pi y ([mk_{y_p}] + j2)/m), \quad (8)$$

where the scaling factor s_c has been defined and the kernel matrixes ρ_1 and ρ_2 are obtained using Eq. (7).

Substitute Eq. (8) into Eq. (4), we have

$$I(x, y) = (s_c(x)s_c(y))^{-1} \sum_{p=1}^M s_p D_p \sum_{j1=-q/2}^{q/2} \sum_{j2=-q/2}^{q/2} \rho_1(j1, k_{x_p}) \rho_2(j2, k_{y_p}) \exp(i2\pi x ([mk_{x_p}] + j1)/m) \times \exp(i2\pi y ([mk_{y_p}] + j2)/m). \quad (9)$$

Let $k1 = [mk_{x_p}] + j1$ and $k2 = [mk_{y_p}] + j1$. Notice that the right part of Eq. (9) can be turned into a form of regular fast inverse Fourier transform on Cartesian coordinate $(k1, k2)$, and then scaled back by $s_c(x)$ and $s_c(y)$, as shown in the following equation.

$$I(x, y) = (s_c(x)s_c(y))^{-1} \sum_{k1=-mN/2}^{mN/2-1} \sum_{k2=-mN/2}^{mN/2-1} \tau_{k1,k2} \exp(i2\pi(xk1 + yk2)/m), \quad (10)$$

where $x, y = [-N/2 : N/2 - 1]/N$. And $\tau_{k1,k2}$ is obtained by rewriting the term of $\sum s_p D_p \sum \sum \rho_1 \rho_2$ in Eq. (9) to the convolution of the weighted k -space data and the kernel matrixes, which is expressed as

$$\tau_{k1,k2} = \sum_{[mk_{x_p}] + j1 = k1} \sum_{[mk_{y_p}] + j2 = k2} s_p D_p \rho_1(j1, k_{x_p}) \rho_2(j2, k_{y_p}), \quad (11)$$

where $p = 1, \dots, M, j1, j2 = -q/2, \dots, q/2$.

In summary, the LS_NUFFT algorithm consists of the following four steps:

1. Generate the kernel matrixes ρ_1 and ρ_2 corresponding to the trajectory k_x, k_y and the scale factor s_c .
2. Obtain convolution $\tau(k1, k2)$ of the weighted k -space data $s_p D_p$ and the kernel matrixes ρ_1 and ρ_2 .
3. Perform 2D FFT on $\tau(k1, k2)$.
4. Re-scale the result by $(s_c(x)s_c(y))^{-1}$.

2.3. Comparison to conventional gridding methods

The Kaiser–Bessel gridding method has been well studied in [3,4]. In this section, the Kaiser–Bessel gridding method is fitted in the framework of the NUFFT by formulating the algorithm using the same configuration of the parameters as that of the LS_NUFFT. The GFFT algorithm is also formulated the same way for comparison. The formulations are shown in Table 1.

Table 1 indicates the principle differences between the LS_NUFFT and the conventional gridding algorithms:

Table 1

Scale factors and kernel matrices for the Kaiser–Bessel (KB), GFFT, and LS_NUFFT algorithms

	KB	GFFT	LS_NUFFT
Scale factor $s_c(x)$	$\frac{\sin(\sqrt{f(x)})}{\sqrt{f(x)}}$	$\exp\left(-b\left(\frac{2\pi x}{m}\right)^2\right)$	$\cos(\pi x/mN)$
Scale factor $s_c(y)$	$\frac{\sin(\sqrt{f(y)})}{\sqrt{f(y)}}$	$\exp\left(-b\left(\frac{2\pi y}{m}\right)^2\right)$	$\cos(\pi y/mN)$
Kernel $\rho_1(j_1, k_{x_p})$	$\frac{I_0(\beta\sqrt{1 - (2(\{mk_{x_p}\} - j_1)/mq)^2})}{q}$	$\exp\left(-\frac{(\{mk_{x_p}\} - j_1)^2}{4b}\right)$	$\mathbf{G}_{j_1,k} a_{k,k_{x_p}}$
Kernel $\rho_2(j_2, k_{y_p})$	$\frac{I_0(\beta\sqrt{1 - (2(\{mk_{y_p}\} - j_2)/mq)^2})}{q}$	$\exp\left(-\frac{(\{mk_{y_p}\} - j_2)^2}{4b}\right)$	$\mathbf{G}_{j_2,k} a_{k,k_{y_p}}$

$f(t) = \pi^2 q^2 t^2 - \beta^2$. I_0 is the first-order modified Bessel function. $x, y = [-N/2 : N/2 - 1]/N$. $j_1, j_2, k = -q/2, \dots, q/2$. $p = 1, \dots, M$. The matrices \mathbf{G} , a and the parameters m, q, N , and M have been defined.

the scale factor and the kernel matrices. By formulating the algorithms using the same configuration of the parameters, it is easier to compare and evaluate the proposed LS_NUFFT with the conventional gridding algorithms.

To further analyze the LS_NUFFT, kernels $\rho_1(j_1, k_{x_p})$ as a function of $\{mk_{x_p}\} - j_1$ for three approaches as defined in Table 1 are illustrated in Fig. 1. It is shown that the kernels of both the Kaiser–Bessel gridding method and the GFFT approach are shift invariant to the trajectory k_{x_p} , yet the LS_NUFFT is shift variant. The Kaiser–Bessel and the GFFT kernel functions do not change their parameters for specific trajectories, however their approximation error is a function of k_{x_p} and k_{y_p} from the perspective of the concept of the NUFFT. Therefore, both the Kaiser–Bessel kernel and GFFT kernel cannot be the best for all trajectories. The LS_NUFFT kernel function enables much more degrees of freedom in the kernel function to fit for every specific trajectory and obtain minimum Least-Square approximation error. Consequently, the LS_NUFFT could lead to more accurate result than that of the Kaiser–Bessel or GFFT kernel functions.

2.4. Computational complexity

Notice that M represents the number of k -space sampling points, N^2 represents the number of pixels in the reconstructed image, the computation complexity for direct summation reconstruction approach is $O(MN^2)$ according to Eq. (4). Typically M is about N^2 . So this complexity is about $O(N^4)$.

For the LS_NUFFT, computation complexity to obtain ρ_1 and ρ_2 is $O(Mq^2)$ according to Eq. (7). The convolution step in Eq.(11) costs $O(Mq^2)$ and the complexity for the 2D FFT step in Eq. (10) is $(mN \log_2(N))^2$. The scaling step by s_c only costs $O(N^2)$ hence can be

ignored. The total complexity is then $O((mN \log_2(N))^2 + Mq^2)$.

Since the conventional gridding method follows the same steps of convolution and 2D FFT, the computational complexity is $O((mN \log_2(N))^2 + Mq^2)$ as well.

Since the computational complexity for LS_NUFFT and conventional gridding method is the same, the reconstruction speed of them is similar as well. Note that usually $m = 2$, $q \leq 8$, $N \geq 64$, the additional computation of the kernel matrix for LS_NUFFT is a minor part as compared with the computation of the 2D FFT and the convolution. In addition, the kernel matrix can be pre-computed for a known trajectory. Consequently the LS_NUFFT does not increase the cost of computation as compared with the conventional gridding method.

3. Experimental assessment

3.1. Methods

Simulations and in vivo experiments were performed to evaluate the reconstruction quality of the LS_NUFFT and conventional gridding method. Experiments were carried out on a GE (Milwaukee, WI) 4T whole body scanner. The FOV was 24 cm, about 1.6 times of the phantom size and the size of the head to avoid aliasing. Both single shot spiral trajectory and four-shot interleaved spiral trajectory were used. The trajectories were designed based on the gradient amplitude and slew rate constrains of the MRI system to enable sufficient image resolution and high sampling speed. Fig. 2 illustrates the 1×4674 k -space trajectory and the DCF for 64×64 pixel images. Other trajectories: $1 \times 13,220$, 4×1168 and 4×3304 are also used but not shown in the figure.

The same trajectories were also used to obtain the k -space phantom data with the mathematical expressions

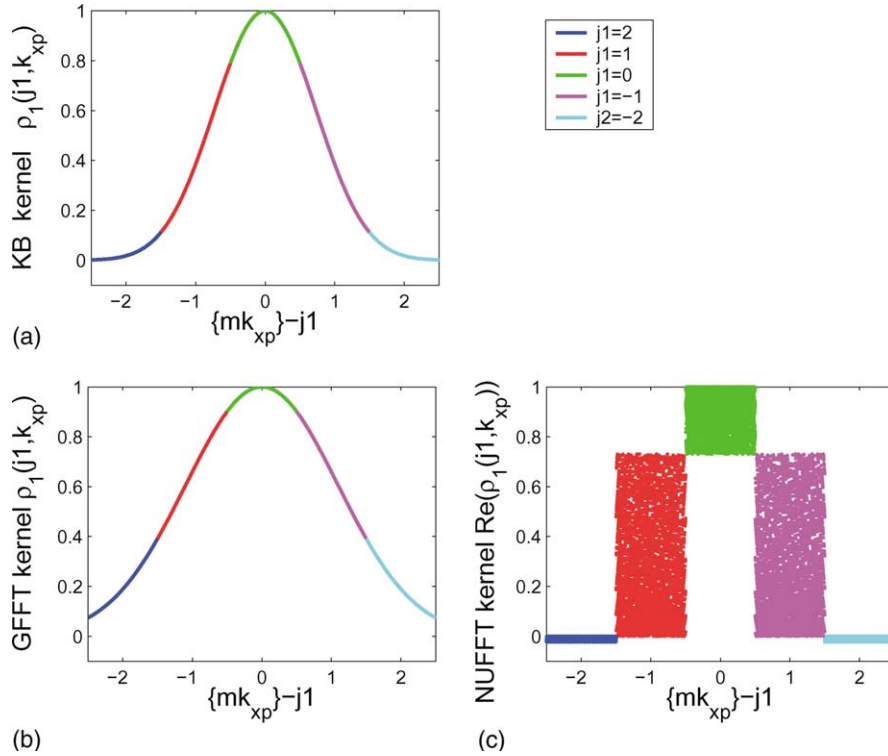


Fig. 1. Illustration of kernels $\rho_1(j_1, k_{xp})$ as a function of $\{mk_{xp}\} - j_1$ (Table 1), assume $m = 2, q = 4$. (a) Kaiser–Bessel, shift (k_{xp}) invariant. (b) GFFT, shift invariant. (c) LS_NUFFT, shift variant, uses a 1×4674 k -space trajectory, 4674 is the number of sampling points. Colors correspond to integer j_1 values.

proposed by Walle et al. in [13]. Two phantoms were considered. One is the Shepp and Logan head phantom, another consists of a set of discs of different radii and intensities superimposed. Both phantoms were slightly smoothed by a Gaussian filter in k -space to suppress ringing artifacts associated with the sharp boundary of the digital phantom, i.e., the high spatial frequency component outside of the finite sampling extends in k -space.

To evaluate the reconstruction results, we used a measure of minimum distance between the images under test and the image reconstructed using direct summation approach. We also compared them directly from

gray-level view and side view. The distance measure is defined as

$$D(I) = \frac{\sqrt{\min_a \|I_d - aI\|^2 / N^2}}{\max(I_d)}, \quad (12)$$

where I is the $N \times N$ image under evaluation, I_d is the reconstructed image using direct summation and a is a variable solved by minimizing the norm term. This measure reflects the approximation error per pixel normalized by the maximum value of the direct summation image. It is so defined to avoid the effect of scaling in amplitude on the evaluation of the reconstructed image, because it does not change the relative contrast of the image, i.e., the information carried by the image.

We use I_n and I_k to represent the image reconstructed using the LS_NUFFT and Kaiser–Bessel gridding method, respectively. All images are assumed taking absolute values.

3.2. Results

Tables 2–4 illustrate the performance of the LS_NUFFT and Kaiser–Bessel gridding method using the measure of $D(I_n)$ and $D(I_k)$ for both 64×64 pixel images and 128×128 images. The noninteger parameter β for Kaiser–Bessel method was optimized using iterative binary search to reach convergence (until the change

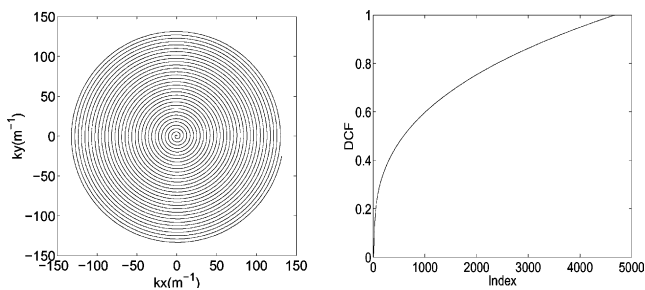


Fig. 2. Left: 1×4674 k -space trajectory, 4674 is the number of sampling points on the trajectory. $(kx, ky) \in [-k_{max}, k_{max}]$, $k_{max} = 133.3$, FOV = 24 cm. Right: density compensation function. It is used for reconstruction of following 64×64 pixel images.

Table 2

Performance evaluation of LS_NUFFT and Kaiser–Bessel (KB) gridding method using the measure of $D(I_n)$ and $D(I_k)$ and digital phantom data

Data(traj, N)	LS_NUFFT	KB	Data(traj, N)	LS_NUFFT	KB
pt1 ($1 \times 4674, 64$)	$1.1e-4$	$1.8e-4$	pt1 ($1 \times 13,220, 128$)	$4.1e-5$	$7.4e-5$
pt2 ($1 \times 4674, 64$)	$8.3e-5$	$1.0e-4$	pt2 ($1 \times 13,220, 128$)	$8.0e-5$	$9.7e-5$

$m = 2, q = 4$ for both methods and $\beta = 30.544$ for Kaiser–Bessel method. pt1 for Shepp and Logan head phantom, pt2 for spot phantom.

Table 3

Performance evaluation of LS_NUFFT and Kaiser–Bessel (KB) gridding method using the measure of $D(I_n)$ and $D(I_k)$ and in vivo experimental data

(traj, N)	LS_NUFFT	KB	(traj, N)	LS_NUFFT	KB
($1 \times 4674, 64$)	$1.7e-4$	$2.6e-4$	($1 \times 13,220, 128$)	$9.2e-5$	$1.2e-4$
($1 \times 4674, 64$)	$1.8e-4$	$2.6e-4$	($1 \times 13,220, 128$)	$9.6e-5$	$1.3e-4$
($1 \times 4674, 64$)	$1.4e-4$	$2.2e-4$	($1 \times 13,220, 128$)	$9.4e-5$	$1.2e-4$
($1 \times 4674, 64$)	$1.4e-4$	$2.2e-4$	($1 \times 13,220, 128$)	$9.4e-5$	$1.2e-4$

$m = 2, q = 4$ for both of them and $\beta = 30.544$ for Kaiser–Bessel method.

Table 4

Performance evaluation of LS_NUFFT and Kaiser–Bessel (KB) gridding method using the measure of $D(I_n)$ and $D(I_k)$ and in vivo experimental data

(traj, N)	LS_NUFFT	KB	(traj, N)	LS_NUFFT	KB
($4 \times 1168, 64$)	$2.3e-4$	$3.3e-4$	($4 \times 3304, 128$)	$1.4e-4$	$2.0e-4$
($4 \times 1168, 64$)	$5.2e-4$	$7.7e-4$	($4 \times 3304, 128$)	$1.4e-4$	$2.0e-4$
($4 \times 1168, 64$)	$1.6e-4$	$2.1e-4$	($4 \times 3304, 128$)	$1.1e-4$	$1.6e-4$
($4 \times 1168, 64$)	$1.7e-4$	$2.2e-4$	($4 \times 3304, 128$)	$1.1e-4$	$1.6e-4$

$m = 2, q = 4$ for both of them and $\beta = 30.544$ for Kaiser–Bessel method.

using D measure is smaller than $1e-8$). The optimal value 30.544 was obtained for the case of $m = 2, q = 4$. This β value differs from Jackson’s β value in [3], largely due to our specific implementation procedure of the

Kaiser–Bessel gridding method to fit it into a consistent framework of NUFFT. Nevertheless, the same formulation as that adopted by Jackson et al. was used, thus our approach should yield the same approximation

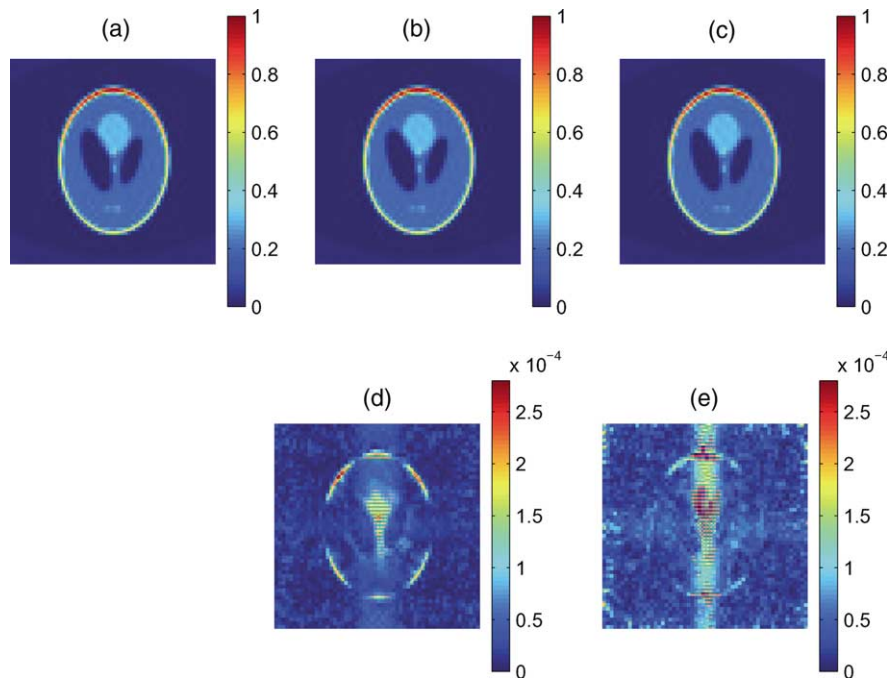


Fig. 3. Performance comparison of the LS_NUFFT and Kaiser–Bessel gridding reconstruction algorithms using head phantom data. (a) Image from direct summation method (I_d). (b) Image from the LS_NUFFT method (I_n). (c) Image from Kaiser–Bessel method (I_k). (d) $Abs(I_d - I_n)$. (e) $Abs(I_d - I_k)$. Use $1 \times 13,220$ spiral out trajectory. $m = 2, q = 4$, and $N = 128$.

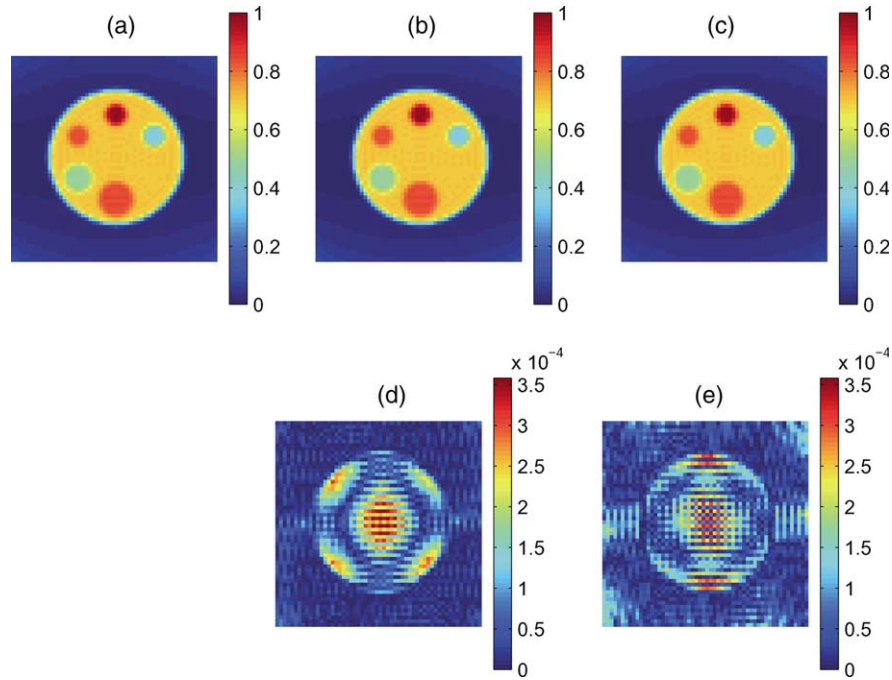


Fig. 4. Comparison of improved nuFFT and Kaiser-Bessel gridding reconstruction using Phantom 2 data. (a) Result from direct summation method. (b) and (e) Result from the LS_NUFFT method. (c) and (f) Result from Kaiser-Bessel method. (d) $Abs(I_d - I_n)$. (e) $Abs(I_d - I_k)$. Use 1×4674 spiral out trajectory. $m = 2$, $q = 4$, and $N = 64$.

error. For different m and q , a new optimization process is needed to obtain a new β . In contrast, the LS_NUFFT is free from the procedure of parameter optimization.

Table 2 illustrates the performance comparisons using digital phantom data. It shows that the distance of the LS_NUFFT image to directly reconstructed image is

consistently smaller ($\approx 30\%$) than that of the Kaiser-Bessel gridding method. And the differences are obvious for the first phantom, which has greater contrast variations within the original image.

Tables 3 and 4 compare the performance of the two algorithms using in vivo experimental data from four

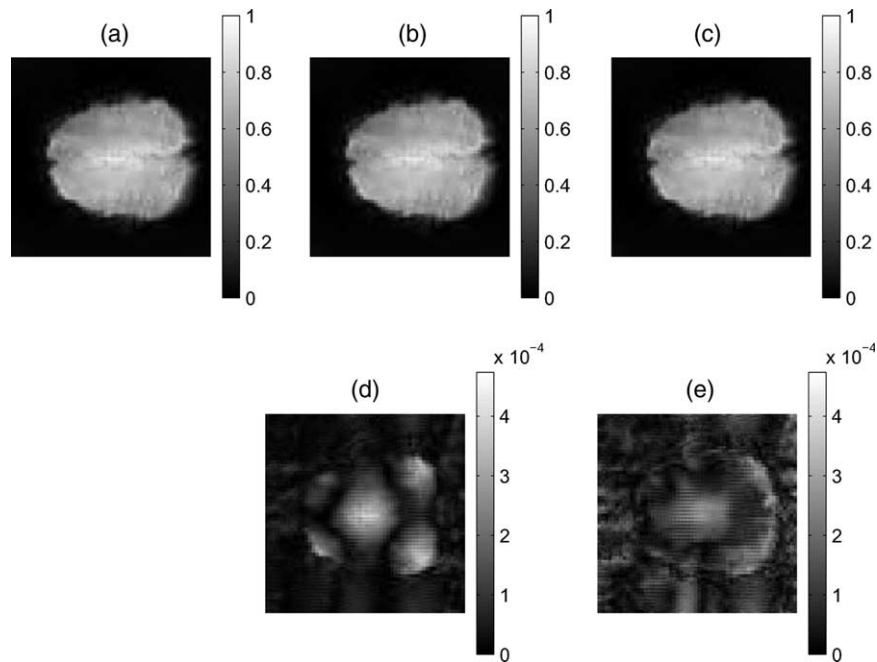


Fig. 5. Comparison of improved nuFFT and Kaiser-Bessel gridding reconstruction using in vivo experiment data. (a) Direct summation I_d . (b) LS_NUFFT I_n . (c) Kaiser-Bessel method I_k . (d) $Abs(I_d - I_n)$. (e) $Abs(I_d - I_k)$. Use $1 \times 13,220$ spiral out trajectory. $m = 2$, $q = 4$, and $N = 128$.

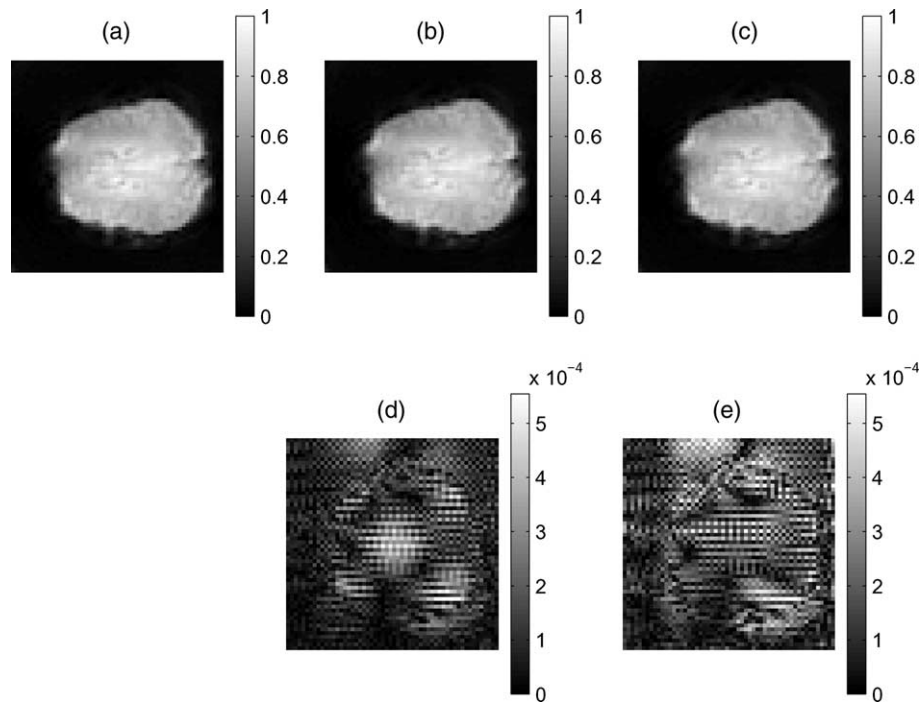


Fig. 6. Comparison of improved nufft and Kaiser–Bessel gridding reconstruction using in vivo experiment data. (a) Direct summation I_d . (b) LS_NUFFT I_n . (c) Kaiser–Bessel method I_k . (d) $\text{Abs}(I_d - I_n)$. (e) $\text{Abs}(I_d - I_k)$. Use 1×4674 spiral out trajectory. $m = 2$, $q = 4$, and $N = 64$.

independent measurements. It is shown that the LS_NUFFT is consistently better for both image sizes and various types of trajectories. It also indicates that the LS_NUFFT is suitable for one shot spiral trajectory.

To demonstrate the result, the reconstructed images are displayed for both phantoms and in vivo experiments. In Fig. 3, reconstructed images from head phantom data with 128×128 size are shown as well as the difference caused by the reconstruction algorithms. It shows that the LS_NUFFT results in a better image with smaller approximation error to the direct summation method than the Kaiser–Bessel method. Fig. 4 demonstrates the advantage of the LS_NUFFT using another phantom with 64×64 size. The improvement of the reconstruction performance by the LS_NUFFT is mainly due to a more explicit solution for the kernel function.

Figs. 5 and 6 strengthen the result using the in vivo experimental data. The differences between the images using Kaiser–Bessel method and the LS_NUFFT to the images using direct summation approach indicate that LS_NUFFT is a better reconstruction method for spiral MRI.

4. Discussion

In general, the LS_NUFFT improves the reconstruction performance of the spiral MRI by generating more explicit kernel functions that fit for the trajectory than conventional shift-invariant kernel functions. And

it is possible to further improve the performance of the LS_NUFFT. For example, better scaling factors can be found to further reduce the approximation error. However, LS_NUFFT has limitation in that it is an approximation to the direct summation reconstruction, which in itself can contain error related to the density compensation function for approximating the nonuniform integration area in the continuous Fourier reconstruction form (Eq. (1)). Recently proposed gridding algorithm, block uniform resampling (BURS) by Rosenfeld [14,15] does not use the same density compensation approximation. It estimates the uniform samples from nonuniform measurements by calculating the local interpolation matrix followed by pseudoinverse operations for each Cartesian grid point. Therefore, the BURS may have performance improvement due to better density compensation as a part of the interpolation step. The idea of integrating improved density compensation into re-gridding procedure may apply to the proposed method to gain additional accuracy. Another advantage of BURS is that it eliminates the 2-1 oversampling which could improve the reconstruction speed when large matrix size is used. However, such reduced sampling scheme may not be applicable in LS_NUFFT because it could degrade the interpolation accuracy of the LS_NUFFT. Nevertheless, the LS_NUFFT, even in its current form, has clear advantages such as straightforward expression for the explicitly optimized kernel function and improved accuracy as compared with conventional method without additional computational cost.

5. Conclusion

An extension of the NUFFT of Liu and Nguyen, called LS_NUFFT, has been proposed to accommodate two-dimensional processes. To assess its accuracy and computational complexity in image reconstruction, comparisons were made with the traditional direct summation method and the conventional Kaiser–Bessel gridding method in the framework of NUFFT.

The reconstructed images from digital phantom data and in vivo experimental data revealed that the LS_NUFFT was more accurate than the Kaiser–Bessel method using the direct summation result as a benchmark. It consistently reduced the reconstruction approximation error. The improvement made by the LS_NUFFT is due to better kernel matrices it generated that fit for the k -space trajectory. It is thus believed that the LS_NUFFT is better than other conventional gridding methods that use ready-made kernel functions. Although this paper is restricted to spiral MRI, the LS_NUFFT can also be useful for other 2D reconstruction applications that collect data on nonuniform spaced points in the transformed domain. It is also worth noting that the new LS_NUFFT technique does not introduce additional computational complexity compared to the conventional Kaiser–Bessel gridding method.

Acknowledgments

The author would like to thank Dr. Gary H. Glover for his software on Kaiser–Bessel reconstruction method and Dr. Ronald Ouwerkerk for his matlab code to generate digital phantom. This work is supported by the grants from the National Science Foundation (BES 0092672) and the National Institutes of Health (NS41328, MH60451).

References

- [1] C. Ahn, J.H. Kim, Z. Cho, High speed spiral scan echo planar imaging, *IEEE Trans. Med. Imaging* 5 (1) (1983) 2–5.
- [2] A. Macovski, C. Meyer, A Novel fast scanning system, in: *Works in Progress, Fifth Annual Meeting of the Society of Magnetic Resonance in Medicine*, 1986, pp. 156–157.
- [3] J. Jackson, C. Meyer, D. Nishimura, A. Macovski, Selection of a convolution function for Fourier inversion using gridding, *IEEE Trans. Med. Imaging* 10 (3) (1991) 473–478.
- [4] J. O'Sullivan, A fast sinc function gridding algorithm for Fourier inversion in computer tomography, *IEEE Trans. Med. Imaging* 4 (MI-4) (1985) 200–207.
- [5] A. Dutt, V. Rokhlin, Fast Fourier transforms for nonequispaced data, *SIAM J. Sci. Comput.* 14 (6) (1993) 1369–1393.
- [6] G. Sarty, R. Bennett, R. Cox, Direct reconstruction of non-Cartesian k -space data using a nonuniform fast Fourier transform, *Magn. Reson. Med.* 45 (2001) 908–915.
- [7] B. Sutton, J. Fessler, D. Noll, A min–max approach to the nonuniform N -dimensional FFT for rapid iterative reconstruction of MR images, *Proc. Int. Soc. Mag. Reson. Med.* 9 (2001) 763.
- [8] Q. Liu, N. Nguyen, An accurate algorithm for nonuniform fast Fourier transforms, *IEEE Microw. Guided Wave Lett.* 8 (1) (1998) 18–20.
- [9] N. Nguyen, Q. Liu, The regular Fourier matrices and nonuniform fast Fourier transforms, *SIAM J. Sci. Comput.* 21 (1) (1999) 283–293.
- [10] V. Rasche, R. Proksa, R.S.P. Börner, H. Eggers, Resampling of data between arbitrary grids using convolution interpolation, *IEEE Trans. Med. Imaging* 18 (1999) 385–392.
- [11] R.H. Remi, K. Kwan, G. Pike, Density compensation functions for spiral MRI, *Magn. Reson. Med.* 38 (1997) 117–128.
- [12] C. Meyer, B. Hu, D. Nishimura, A. Macovski, Fast spiral coronary artery imaging, *Magn. Reson.* 28 (1992) 202–213.
- [13] R. Walle, H. Barrett, K. Myers, M. etc, Reconstruction of MR images from data acquired on a general nonregular grid by pseudoinverse calculation, *IEEE Trans. Med. Imaging* 19 (12) (2000) 1160–1167.
- [14] D. Rosenfeld, An optimal and efficient new gridding algorithm using singular value decomposition, *Magn. Reson. Med.* 40 (1998) 14–23.
- [15] D. Rosenfeld, New approach to gridding using regularization and estimation theory, *Magn. Reson. Med.* 48 (2002) 193–202.